3340 *Macromolecules* **2010**, *43*, 3340–3351
DOI: 10.1021/ma902564b

Macromolecules
ARTICLE

From Rouse to Fully Established Entanglement Dynamics: A Study of Polyisoprene by Dielectric Spectroscopy

A. Abou Elfadl,[†] R. Kahlau,[†] A. Herrmann,[†] V. N. Novikov,[‡] and E. A. Rössler*[,†]

[†]*Experimentalphysik II, Universität Bayreuth, 95440 Bayreuth, Germany, and* [‡]*IA&E, Russian Academy of Sciences, Novosibirsk 630090, Russia*

Received November 20, 2009; Revised Manuscript Received February 19, 2010

ABSTRACT: Polyisoprenes (PI) covering a wide range of molecular weights (M in g/mol) from $652 \leq M \leq 4.36 \times 10^5$ are investigated by dielectric spectroscopy. Normal mode (τ_n) and segmental (or α-) relaxation (τ_α) are considered. The normal mode spectra are singled out by subtracting the spectra of the segmental relaxation. This yields the full spectrum including its high-frequency cutoff. Regarding the Rouse regime ($1040 < M < 9910 \cong M_c \cong 2M_e$), we are able to construct a master curve which is quantitatively reproduced by the Rouse theory provided that a weak stretching ($\beta_K = 0.8$) of the correlation function is introduced for each mode. In the low M limit ($M < 1040$) the normal mode can not any longer be clearly identified. In the entanglement regime ($M > M_c$) the normal mode spectrum exhibits a power-law behavior $\varepsilon'' \propto \nu^{-\gamma}$ at high frequencies with an exponent continuously changing until it saturates around $M_r \cong 10^5$, yielding $\gamma = 0.26 \pm 0.01$. Moreover, the M dependence of the ratio τ_n/τ_α changes from $M^{4.0}$ at $M_c < M < M_r$ to $M^{3.0}$ at $M > M_r$. The latter exponent is that of pure tube reptation; yet, the exponent $\gamma = 0.26$ is not compatible with the reptation model. Nevertheless, both findings we take as evidence for another characteristic molecular weight, namely, $M_r \cong 20M_e$, beyond which entanglement dynamics are fully established. Analyzing the strength of the normal mode relaxation as a function of M yields Gaussian statistics of the chains at $M > 2000$, i.e., well below M_c. Including data from field cycling NMR, we provide master curves for both the segmental as well as the terminal relaxation time as a function of $T - T_g$, where T_g denotes the glass transition temperature.

I. Introduction

Understanding the microscopic dynamics of melts of linear polymers still remains a challenge. Two theoretical models are discussed accounting for the long-range dynamics in polymers, namely, the Rouse model of unentangled polymers ($M < M_e$) and the tube-reptation model for entangled polymers ($M > M_e$).[1−6] Here, M_e denotes the entanglement molecular weight, i.e., the molecular weight (M) above which entanglement effects are expected to dominate the dynamics at long times. At very short times, "segmental" or "local" relaxations occur. As the polymer constitutes a viscous medium the segmental dynamics is in fact dominated by that of the glass transition phenomenon, which itself includes cooperative motion.[7−9] Consequently, the segmental correlation time τ_s may be identified with that of the α-process, τ_α, characterizing the glass transition. The latter drives the polymer dynamics via determining the monomeric friction coefficient and is responsible for the non-Arrhenius temperature dependence of the relaxation times in polymer melts.

Several experimental techniques[10−18] as well as simulation studies[19−27] have tackled the problem of identifying the microscopic dynamics in polymers. Yet, the full microscopic correlation function reflecting segmental, Rouse, and reptation dynamics is still not completely known. For example, studying the crossover from Rouse to reptation dynamics in terms of the bond vector correlation function, Monte Carlo simulations by Kreer et al.[20] as well as recent fast field cycling (FFC) NMR by Herrmann et al.[18] have not found the crossover to the predicted power-law behavior of the tube-reptation model. Among others,[5] the authors speculated that the crossover might be highly protracted being reached only at very high M, i.e., at $M \gg M_e$.

*Corresponding author.

A technique that allows studying polymer dynamics and segmental dynamics is offered by dielectric spectroscopy (DS) using type A polymers.[10,12,13,28−31] Such polymers contain a component of the monomeric dipole moment along the chain contour usually in addition to a component perpendicular to the chain. The first component gives rise to the normal mode relaxation and reflects the fluctuation spectrum of the end-to-end vector, whereas the latter component yields information on the segmental dynamics.[10,29,30] In other words, DS provides the exceptional chance to investigate both segmental and long-range polymer dynamics simultaneously. (Here, we note that in our previous works, following Lunkenheimer et al.,[8] the segmental dynamics has been called "glassy dynamics".)

Here, we study the dielectric relaxation behavior of linear *cis*-1,4-polyisoprene (PI), a type A polymer well studied by DS.[11,32−36] Yet, there are several points not completely clarified. (i) Although Rouse theory applies in fair approximation for the unentangled polyisoprene, systematic deviations are observed which deserve quantification. (ii) The spectral shape of the normal mode relaxation is not fully understood and/or controversially discussed when crossing from the unentangled to the entangled polymer regime.[3,29,32] (iii) Within the tube-reptation model, free Rouse dynamics are also expected for entangled polymers at $\tau_s < t < \tau_e$, where τ_e denotes the entanglement time at which first constraints from tube formation are felt by the chain.[2,3] This is not well tested by DS. (iv) As the tube-reptation model does not fully account for all experimental findings, it is argued that it may work the better the longer the chains are, i.e., at such high M for which additional topological fluctuations may be more and more neglected.[5,6] Thus, not only the crossover at $M_c \cong 2M_e$ is of relevance but also a possible change of the M dependence of the normal mode relaxation time at highest M. (v) The crossover to

 Published on Web 03/05/2010

Table 1. Molecular Weights (M) of the *cis*-1,4-Polyisoprenes (PI) Studied: Weight-Average M_w, Number-Average M_n, and Polydispersity M_w/M_n (Sample Name Indicates M_w)

name	M_w [g/mol]	M_n [g/mol]	M_w/M_n	temperature range investigated [K]
PI 652	6.52×10^2	5.93×10^2	1.1	175−313
PI 790	7.90×10^2	7.07×10^2	1.12	175−343
PI 1040	1.04×10^3	9.50×10^2	1.09	175−363
PI 1370	1.37×10^3	1.26×10^3	1.09	195−363
PI 1920	1.92×10^3	1.79×10^3	1.07	190−353
PI 3840	3.84×10^3	3.62×10^3	1.05	195−363
PI 4470	4.47×10^3	4.31×10^3	1.04	199−373
PI 9910	9.91×10^3	9.73×10^3	1.02	199−353
PI 13500	1.35×10^4	1.32×10^4	1.02	200−363
PI 14900	1.49×10^4	1.46×10^4	1.02	200−373
PI 21200	2.12×10^4	2.07×10^4	1.03	200−363
PI 47300	4.73×10^4	4.69×10^4	1.01	180−373
PI 110000	1.10×10^5	1.09×10^5	1.01	200−393
PI 157000	1.57×10^5	1.55×10^5	1.01	200−393
PI 314000	3.14×10^5	3.04×10^5	1.03	213−363
PI 436000	4.36×10^5	4.25×10^5	1.03	173−373

the behavior of a simple liquid without any polymer dynamics is not well documented. More explicitly, where does the normal mode relaxation disappear when the polymer chain becomes shorter and shorter? Recent FFC NMR studies have shown that in the case of polybutadiene (PB) at M (in g/mol) < 500 no polymer specific relaxation is found;[17] such oligomers behave like simple liquids, more precisely like simple glass-formers, and consequently the molecular weight of the Rouse subchain or Rouse unit has been taken to be around $M_R \cong 500$ in the case of PB.

In the present contribution, we investigate a series of PI in the molecular weight range $652 < M < 4.36 \times 10^5$ (cf. Table 1) and attempt to address the above raised questions. We mention that the crossover molecular weight $M_c \cong 2M_e$ of PI is found by DS to be around 10^4.[3,29,37] In addition to analyzing the Rouse regime, the evolution of the spectral shape of the normal mode relaxation will be considered when passing through M_e and reaching very high M values. We will demonstrate that an M-independent normal mode spectrum is only obtained at $M > 10^5$, which is actually much higher than M_e. This is accompanied by a change of the M dependence of the terminal relaxation time; specifically, its power-law exponent is 4.0 at $M_c < M < 10^5$ but returns to 3.0 for $M > 10^5$. In other words, the crossover to fully developed entanglement dynamics turns out to be highly protracted in agreement with previous NMR[18] and simulation work.[20]

II. Theoretical Background: Dielectric Relaxation Analyzed within the Frame of the Rouse Theory

The present work deals with the dielectric response of a type A polymer, namely polyisoprene (PI). In this case two relaxations are observed: the segmental (or α-relaxation) determined by the dynamics of the glass transition and a second low-frequency relaxation, the normal mode relaxation, originating from the collective polymer dynamics.[12,13,29,30] Generally, the dielectric permittivity is defined by the equation[38,39]

$$\varepsilon^*(\omega) = \varepsilon'(\omega) - i\varepsilon''(\omega) = \varepsilon_\infty + \Delta\varepsilon \int_0^\infty -\frac{d\phi(t)}{dt} e^{-i\omega t}\, dt \quad (1)$$

where $\varepsilon^*(\omega)$ is the complex dielectric constant, ω is the angular frequency, and ε_∞ is the high-frequency permittivity. The step response function $\phi(t)$ may be identified with the microscopic dipole correlation if internal field effects can be ignored, which actually holds well for polymers with low polarity such as PI.[41] Regarding the segmental dynamics, the step response function $\phi(t) = \phi_\alpha(t)$ is described by some stretched relaxation function. Here, for interpolating the corresponding spectrum $\varepsilon''(\omega)$, we will apply as often done[30] the Havriliak−Negami (HN) susceptibility function.[40]

$$\varepsilon^* - \varepsilon_\infty = \Delta\varepsilon / [1 + (i\omega\tau_s)^{1-a}]^b \quad (2)$$

where τ_s is the nominal relaxation time, a and b are the shape parameters ($0 \le a, b \le 1$), describing the high- and low-frequency broadening of the dispersion. Then, in terms of apparent power laws the dielectric loss is characterized by $\varepsilon''(\nu) \propto \nu^\alpha$ ($\nu \ll \nu_{max}$) and $\varepsilon''(\nu) \propto \nu^{-\beta}$ ($\nu \gg \nu_{max}$), where ν_{max} denotes the frequency of the relaxation maximum and the HN parameters a and b are related to the apparent shape parameters by $\alpha = (1 - a)$ and $\beta = (1 - a)b$.[38]

In the case of the normal mode relaxation, $\phi(t) = \phi_n(t)$ is given by the autocorrelation function of the end-to-end vector $\mathbf{R}$ of a polymer chain[13,29,30]

$$\phi(t) = \frac{\langle \mathbf{R}(t) \cdot \mathbf{R}(0) \rangle}{\langle \mathbf{R}(0)^2 \rangle} \quad (3)$$

We note that at short times close to segmental relaxation times a possible cross-term of the correlation between the components of the dipole moment along and perpendicular to the chain may give a contribution to the relaxation spectrum. A possible existence of this contribution may obscure to some extent the analysis of the spectral shape in the region where the segmental and normal mode relaxations overlap. Here, we neglect these terms. Possibly, the non-Debye behavior for $\omega\tau_s \ll 1$ of the HN function may reflect these cross-terms.

In the polymer melt, the dynamics of relatively short, nonentangled polymer chains may be described by the Rouse model.[2,41] It is assumed that the chains are Gaussian and sufficiently long, so that they can be further subdivided into Gaussian segments. The chain is then represented by N "beads" of mass M_R, immersed in an effective viscous medium and connected by $N - 1$ mass-less entropic springs. It is assumed that viscous damping is sufficiently large, so that inertial effects are negligible. Solving the corresponding eigenvalue problem for a chain then yields N orthogonal relaxation modes $p = 0, 1, ..., N - 1$ ($p = 0$ corresponds to uniform translation not considered here) with relaxation times (eigenvalues) τ_p and normal coordinates (eigenvectors) $\mathbf{X}_p(t)$, the so-called Rouse modes

$$\mathbf{X}_p(t) = \frac{1}{N} \sum_{n=1}^{N-1} \mathbf{R}_n(t) \cos \frac{p\pi(n - 1/2)}{N} \quad (4)$$

where $\mathbf{R}_n(t)$ is the position vector of nth bead. The correlation functions of Rouse normal modes $\mathbf{X}_p(t)$ are then[42,43]

$$C_p(t) = \langle \mathbf{X}_p(t)\cdot\mathbf{X}_p(0)\rangle = \frac{b^2}{8N\sin^2(p\pi/2N)}\exp(-t/\tau_p) \qquad p = 1, ..., N-1 \quad (5)$$

where b is the effective Rouse segment length. The relaxation time τ_p of the pth mode is

$$\tau_p = \frac{\tau_0\pi^2}{4\sin^2(p\pi/2N)} \quad (6)$$

with $\tau_0 = b^2\zeta/(3\pi^2kT)$, where ζ is the friction coefficient of a bead. The longest relaxation time τ_R, the so-called Rouse time, corresponding to $p = 1$, is then given by

$$\tau_R = \frac{\tau_0\pi^2}{4\sin^2(\pi/2N)} \quad (7)$$

For long chains with $N \gg 1$, the essential part of the polymer dynamics comes from the modes with $p/N \ll 1$. In this case, the sine in eqs 5−7 can be substituted by its argument, and then the parameters of the Rouse dynamics have the form most often found in the literature[2,3,29]

$$C_p(t) \approx \frac{Nb^2}{2\pi^2p^2}\exp(-t/\tau_p), \quad \tau_p \cong \tau_0N^2/p^2 \quad \text{and } \tau_R \cong \tau_0N^2 \quad (1 \le p \le N) \quad (8)$$

This so-called continuous Rouse model is, however, a poor approximation for relatively short chains with only a few Rouse modes. We therefore use the exact eqs 6 and 7 in the following and refer to it as the discrete Rouse model.[17,42]

The end-to-end vector in eq 3 in terms of the Rouse model is equal to $\mathbf{R}(t) = \mathbf{R}_N(t) - \mathbf{R}_1(t)$. Expressing $\mathbf{R}_n(t)$ via the normal modes $\mathbf{X}_p(t)$

$$\mathbf{R}_n(t) = \mathbf{X}_0(t) + 2\sum_{p=1}^{N-1}\mathbf{X}_p(t)\cos\frac{p\pi(n-1/2)}{N} \quad (9)$$

one obtains

$$\mathbf{R}_N(t) - \mathbf{R}_1(t) = 2\sum_{p=1}^{N-1}\mathbf{X}_p(t)[\cos p\pi(1-1/2N) - \cos p\pi/2N] \quad (10)$$

and

$$\langle \mathbf{R}(t)\cdot\mathbf{R}(0)\rangle = 16\sum_{p,q=1}^{N-1}\langle \mathbf{X}_p(t)\cdot\mathbf{X}_q(0)\rangle\cos\left(\frac{p\pi}{2N}\right)\cos\left(\frac{q\pi}{2N}\right)\sin^2\left(\frac{p\pi}{2}\right)\sin^2\left(\frac{q\pi}{2}\right) \quad (11)$$

Taking into account that the mixed normal mode correlation functions ($q \neq p$) vanish and substituting $\langle \mathbf{X}_p(t)\cdot\mathbf{X}_p(0)\rangle$ from eq 5 yields

$$\langle \mathbf{R}(t)\cdot\mathbf{R}(0)\rangle = \frac{2b^2}{N}\sum_{p=1,3,...}^{N-1}\cot^2\left(\frac{p\pi}{2N}\right)\exp(-t/\tau_p) \approx \frac{8b^2N}{\pi^2}\sum_{p=1,3,...}^{N-1}\frac{1}{p^2}\exp(-t/\tau_p) \quad (12)$$

As indicated, the summation index includes now only odd integers. The last equation represents again the limit of the continuous Rouse model and shows that in the dielectric response the polymer modes with smallest p, i.e., slowest Rouse modes, are dominating. Finally, from eq 1 we have

$$\varepsilon''(\omega) = \Delta\varepsilon_n\omega\int_0^\infty \mathrm{d}t\,\phi_n(t)\cos\omega t \quad (13)$$

where

$$\phi_n(t) = \frac{2}{N(N-1)}\sum_{p=1,3,...}^{N-1}\cot^2\left(\frac{p\pi}{2N}\right)\exp(-t/\tau_p) \quad (14)$$

$\Delta\varepsilon_n$ is the relaxation strength of the normal mode spectrum, and we took into account that

$$\sum_{p=1,3,...}^{N-1}\cot^2\left(\frac{p\pi}{2N}\right) = \frac{N(N-1)}{2}$$

As a result, one finally finds

$$\varepsilon''(\omega) = \frac{2\Delta\varepsilon_n}{N(N-1)}\sum_{p=1,3,...}^{N-1}\cot^2\left(\frac{p\pi}{2N}\right)\frac{\omega\tau_p}{1+(\omega\tau_p)^2} \quad (15)$$

Figure 1a displays the normal mode susceptibility $\chi_n''(\omega\tau_s) = \varepsilon''(\omega\tau_s)/\Delta\varepsilon_n$ calculated from eq 15 for a number of different N. The time constant $\tau_0 = \tau_s$ is the segmental time, and it may tentatively be identified with τ_α as obtained from analyzing the segmental or α-relaxation peak. The spectra are characterized by a low-frequency peak with a frequency given by eq 7 and a Debye-like cutoff at high frequencies; specifically, the shortest time is $\tau_{N-1} = \tau_s\pi^2/2 \approx 4.9\tau_s$ (cf. eq 6). In between a power-law regime $\varepsilon''(\omega) \propto \omega^{-\gamma}$ develops with an exponent reaching $\gamma = 0.5$ for high N, say at $N > 20$.

The Rouse spectra calculated in Figure 1a may be vertically shifted to yield a common envelope in the frequency range $\omega\tau_n \ll \omega\tau_s \ll 1$. This is shown in Figure 1b where the quantity $\chi_n''(\omega)\langle R^2(0)\rangle/b^2$ is plotted (cf. eq 12). Clearly, the envelope is well recognized, and this representation allows to check whether the Rouse theory is applicable for the experimental data. In the discrete model, the corresponding shift factor is $SF = \langle R^2(0)\rangle/b^2 = N - 1$ as follows from eq 12 because the sum at $t = 0$ is equal to $N(N-1)/2$.

Actually, as revealed in particular by simulations,[20−25] a Rouse mode correlation function may depend on time as a stretched exponential with a stretching parameter $\beta_K(p)$. Thus, we phenomenologically generalize eq 14 to

$$\phi_n(t) = \frac{2}{N(N-1)}\sum_{p=1,3,...}^{N-1}\cot^2\left(\frac{p\pi}{2N}\right)\exp\left[-(t/\tau_p)^{\beta_K(p)}\right] \quad (16)$$

and take it as an empirical fit function.

Finally, as the relaxation strength of the normal mode spectrum is given by

$$\Delta\varepsilon_n = nR_e^2(4\pi\mu^2/3kT) \quad (17)$$

with n being the chain number density, $R_e^2 = Nb^2$ the mean-square end-to-end distance of the chain, and μ the magnitude of monomeric dipole moment along the chain contour,[29] we expect that $\Delta\varepsilon_n \propto nR_e^2$, which becomes independent of N if Gaussian statistics have fully developed; specifically, $R_e^2 \propto N$ and $n \propto N^{-1}$ in this limit.

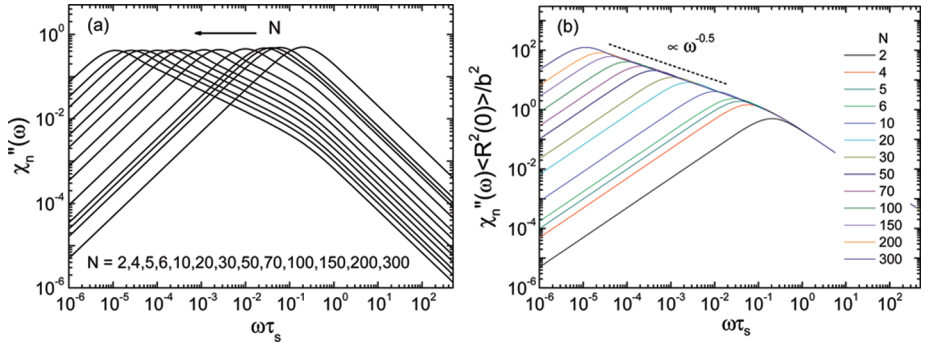

Figure 1. (a) Dielectric susceptibility (normal mode spectrum) calculated for the discrete Rouse model; τ_s denotes the segmental time constant. (b) Data as in (a) but multiplied with $\langle R^2(0)\rangle/b^2$ to provide a common envelope.

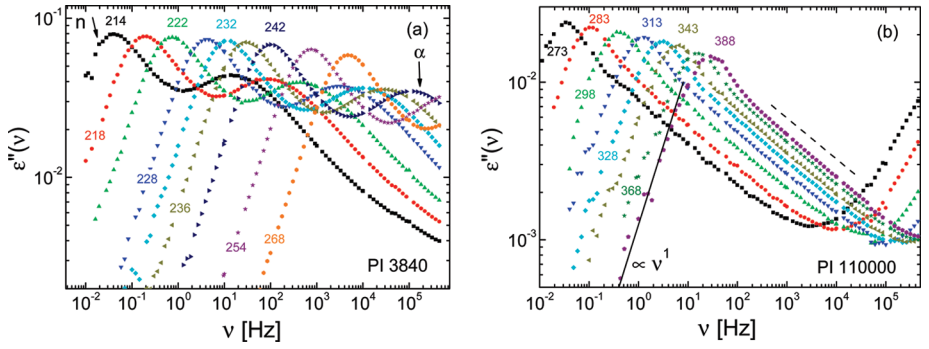

Figure 2. (a) Dielectric spectra of polyisoprene (PI) with $M = 3840$ at different temperatures; both normal (n) and α-relaxation peaks (α) are observed. (b) Dielectric spectra of PI with $M = 1.10 \times 10^5$; only normal mode relaxation resolved. Solid line: Debye behavior $\varepsilon''(\nu) \propto \nu^1$; dashed line: high-frequency power-law behavior $\varepsilon''(\nu) \propto \nu^{-\gamma}$ with $0 < \gamma < 1$.

Here a note is worthwhile. In contrast to the type A model chain assumed in the theory with a cumulative dipole moment along the entire chain, real chain molecules like polyisoprene cannot be prepared with only a single configuration. Here, the cis configuration is interrupted by trans and vinyl configurations. This may change the end-to-end vector **R**, but still the cumulative dipole moment is expected to be proportional to **R**, thus allowing to probe polymer dynamics.

III. Experimental Section

Broad-band dielectric spectra were measured by applying an Alpha-A spectrometer from Novocontrol. The setup covered a frequency range of $10^{-2}-10^6$ Hz. The dielectric cell is constructed according to a design by Wagner and Richert[44] and made out of gold-plated Invar steel to provide thermal invariance of the capacity (diameter 18 mm and $C_0 \cong 40$ pF). The filled dielectric cell was inserted in an Oxford cryostat for which temperature control was provided by a Novocontrol Quatro system. Temperature stability was better than 0.1 K.

Standard *cis*-1,4-polyisoprene (PI) samples with weight-average molecular weight M_w (in g/mol) in the range $652-4.36 \times 10^5$ and with polydispersity $M_w/M_n = 1.01-1.12$ were purchased from Polymer Standards Service (PSS), Mainz, Germany, and used without further purification. The polymers were synthesized in *n*-hexane solution with *sec*-butylithium as initiator and bear the two end groups, *sec*-butyl and H. According to the supplier, the microstructure contains 66% cis, 27% trans, and 7% vinyl configuration. At low M this distribution may somewhat change. The molecular weights M_w and M_n were determined by PSS from the molecular weight distribution obtained by gel permeation chromatography (GPC). The measurements were performed on an apparatus equipped with analytical columns PSS SDV (with a particle size of 5 μm) at 23 °C with THF as solvent and flow rate 1 mL/min using a refractive index detector (Shodex RI 71 or Agilent RI). By checking M for some of the purchased samples through on-site GPC, we find an error of about 10% (23 °C; solvent: THF; flow rate 1 mL/min; PSS SDV 5 μm columns; detectors: Shodex RI-101, Waters 410 RI, Waters 486 UV). The samples were put in a vacuum oven for 24 h at room temperature to remove possible oxygen and residual solvent. Molecular weight M_w, number-average molecular weight M_n, and polydispersity M_w/M_n of each sample are listed in Table 1. The sample name indicates the weight-average M in g/mol.

IV. Results

Dielectric Spectra. Typical DS spectra are shown for PI 3840 in Figure 2a. Clearly, two relaxation peaks are observed. The larger peak at lower frequencies is attributed to the normal mode relaxation (*n*) and the smaller peak at higher frequencies to the segmental relaxation or α-process (α). On the high-frequency flank of the α-process a crossover to an "excess wing" is discernible and attributed to secondary relaxation processes well-known from low molecular weight glass-formers.[8,9,30,45−47] Figure 2b displays the spectrum of PI 110000, a system with high M for which α-process and normal mode relaxation are well separated. Here and for most other high-M spectra the dc conductivity was removed by assuming a power-law contribution of the kind $\varepsilon''(\nu) = \sigma_{dc}/(2\pi\varepsilon_0\nu)$ (cf. Figure 19 in the Appendix). The normal mode peak is observed at low frequencies while only at highest frequencies the onset of the α-process is observed. In between a high-frequency flank of the normal mode peak is recognized which can be described by a power law $\varepsilon''(\nu) \propto \nu^{-\gamma}$ with $0 < \gamma < 1$. In all the spectra the low-frequency flank of the normal mode peak exhibits a Debye-behavior; i.e., it follows a power law $\varepsilon''(\nu) \propto \nu^1$. The spectra measured exhibit all the features well-known from other studies on PI.[11,30,32−35]

In Figure 3a, a selection of spectra for PI 790 is plotted. In this low-M limit, the double-peak character of the spectra

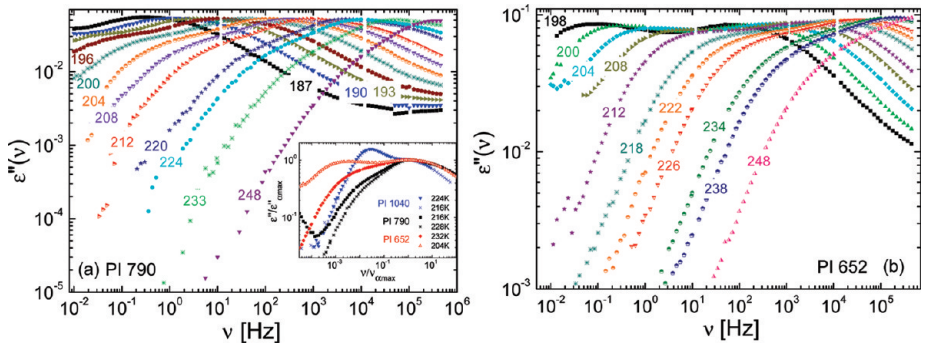

Figure 3. (a) Dielectric spectra of polyisoprene (PI) with $M = 790$. (b) Corresponding spectra of PI with $M = 652$. Inset in (a): spectra of PI 1040, PI 790, and PI 652 rescaled by the height and the position of the peak at highest frequencies.

has essentially disappeared. A broad peak is recognized with some indication of a low-frequency shoulder not changing significantly its amplitude. The shoulder could be a reminiscence of very weak normal mode relaxation. Figure 3b displays typical spectra of PI 652, i.e., for an even shorter PI chain. Here, two relaxation peaks are resolved at low temperatures. With increasing temperature, the high-frequency peak grows on the expense of the low-frequency peak and the two peaks approach each other. Both sets of spectra cannot be easily interpreted. The polydispersity is somewhat larger than for the other samples (cf. Table 1), and the microstructure may be different. In particular, in the case of PI 652, the spectral evolution resembles the interplay of α-relaxation and a secondary (β) relaxation known for amorphous polymers[9,28,30,47] and low-molecular-weight glass-formers.[9,47,48] In the inset of Figure 3a, selected spectra of PI 652, PI 790, and PI 1040 are displayed rescaled to collapse in the frequency range of the main relaxation peak at highest frequencies. For PI 652 and PI 790, the spectral separation between the main peak and the low-frequency shoulder is larger than in the case of PI 1040. Thus, any systematic M dependence of the relaxation behavior is lost for $M < 1040$, and it is not at all clear whether the low-frequency shoulder may be attributed to a normal mode process. Hence, we refrain to draw any further conclusion.

In order to illustrate the change of the spectral shape of the normal mode as well as of the α-relaxation with temperature, we show in Figure 4a spectra of PI 3840, for which $\varepsilon''(\omega)/\varepsilon''_{\mathrm{nmax}}$ is plotted versus the rescaled frequency ν/ν_{nmax}, where $\varepsilon''_{\mathrm{nmax}}$ and ν_{nmax} denote the height and the frequency, respectively, of the normal mode peak. In the frequency range of the normal mode relaxation the data agree well but not in the range of the α-process, indicating that frequency−temperature superposition (FTS) applies for the normal mode spectra but not for the complete response; i.e., in general, normal mode and α-relaxation have different temperature dependences. However, inspecting only high-temperature data (cf. inset in Figure 4a), FTS works very well for the full spectrum. Figure 4b displays the so rescaled data for the frequency range of normal mode relaxation of PI 110000. A master curve is found for which the high-frequency flank is described by a power law with $\gamma = 0.26$. Regarding the α-process, Figure 4c presents analogously rescaled spectra, $\varepsilon''(\omega)/\varepsilon''_{\alpha\mathrm{max}}$ vs $\nu/\nu_{\alpha\mathrm{max}}$, for high temperatures. Whereas FTS applies at high temperatures, it appears to fail again at low temperatures (cf. inset in Figure 4c). Surprisingly, the α-peak becomes narrower at low temperatures. Similar results were reported by Adachi et al.[33] In Figure 19 (Appendix) we show the master curve for PI 314000 for which normal mode and α-relaxation are separated too much to test full FTS; yet, for each individual relaxation FTS works well provided that one discards the secondary process at highest frequencies.

Concerning the M dependence of the spectra, rescaled data $\varepsilon''(\nu)/\varepsilon''_{\alpha\mathrm{max}}$ versus $\nu/\nu_{\alpha\mathrm{max}}$ are displayed in Figure 5 for the high-temperature range, i.e., for temperatures for which FTS applies for the total spectra and consequently coinciding curves for a given M are observed for the temperature range indicated in Figure 5. As is also shown in Figure 16b (inset), the ratio $\nu_{\alpha\mathrm{max}}/\nu_{\mathrm{nmax}} = \tau_{\mathrm{n}}/\tau_{\alpha}$ becomes temperature independent for $T > T_{\mathrm{g}} + 35$ K with T_{g} denoting the glass transition temperature. As expected, for higher M the normal mode peak shifts to lower reduced frequencies. Once again, one sees that the envelope of the α-spectra is temperature as well as M independent. Two samples, namely PI 21200 and PI 13500, show some deviations regarding the height of the normal mode peak with respect to the others for reasons not known. The temperature independent ratio $\nu_{\alpha\mathrm{max}}/\nu_{\mathrm{nmax}} = \tau_{\mathrm{n}}/\tau_{\alpha}$ ($T > T_{\mathrm{g}} + 35$ K) is displayed as a function of M in Figure 6. By plotting this ratio (instead of solely $1/\nu_{\mathrm{nmax}}$ at a fixed temperature), the M dependence of the monomeric friction coefficient which drives the temperature dependence of τ_{n} and is given by that of the segmental dynamics (cf. Figure 15a) is accounted for. This approach provides an "isofrictional"[43] representation of the data. In most DS studies this has not been taken into account. In the case of the four samples with $M = 1.10 \times 10^5 - 4.36 \times 10^5$, for which both relaxation peaks cannot be observed in a single spectrum, $\nu_{\alpha\mathrm{max}}$ was obtained by extrapolating along the master curve $\tau_{\alpha} = f(T - T_{\mathrm{g}})$ (cf. below and Figure 16a). Three power-law regimes (I−III) are recognized in Figure 6, specifically $\tau_{\mathrm{n}}/\tau_{\alpha} \propto M^{d}$, with the exponents $d_{\mathrm{I}}' = 2.6$, $d_{\mathrm{II}} = 4.0$, and $d_{\mathrm{III}} = 3.0$. Note that the apparent exponent d_{I}' for regime I decreases when considering the normal mode spectra after subtracting the α-peak (see below). The first crossover (I, II) is compatible with attributing the entanglement molecular weight to $M_{\mathrm{c}} \cong 10^4$,[3,29,37] above which entanglement dynamics dominate whereas below Rouse dynamics of unentangled chains are found (cf. also below).[1,29,30] Similar results for PI were reported by others.[11,32,34,37] The second crossover (II, III) has not been reported before. Here, the exponent d returns to a lower value which in fact is that of the pure tube-reptation model.[2] Below we will show evidence that also the changes of the normal mode spectrum saturate only above $M \cong 10^5$.

Spectral Shape of the Normal Mode Relaxation. In Figure 7 we collapsed high-temperature spectra for all M in such way to scale the minimum between normal mode and α-relaxation; i.e., in this representation the spectra show the same minimum by height and position. In the regime $M \leq 9910$ (data marked green), the flanks of the minimum can be interpolated in fair approximation by a sum of two power

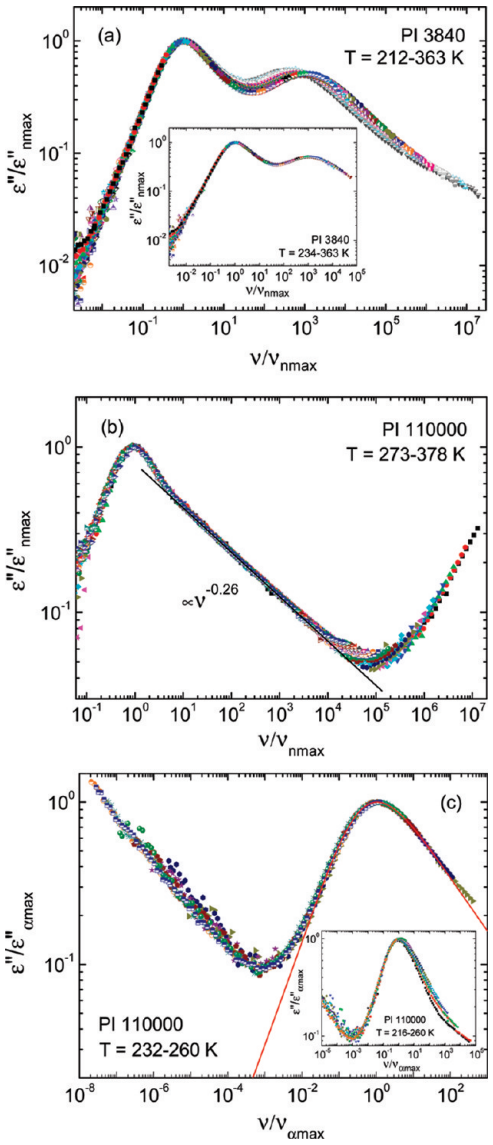

Figure 4. (a) Rescaled dielectric spectra of polyisoprene (PI) with M = 3840 for all temperatures measured; $\varepsilon''(\nu)$ is rescaled by the maximum height $\varepsilon''_{\mathrm{nmax}}$ and ν by the frequency ν_{nmax} of the normal mode peak. Inset: highest temperatures only. (b) Analogous plot for of PI with $M = 1.10 \times 10^5$. (c) High-temperature data for PI with $M = 1.10 \times 10^5$ and $\varepsilon''(\nu)$ rescaled by the maximum height $\varepsilon''_{\alpha\mathrm{max}}$ and by the frequency $\nu_{\alpha\mathrm{max}}$ of the α-peak. Solid line: HN fit with $a = 0.3$ and $b = 0.52$ corresponding to the apparent exponents $\alpha = 0.70$ and $\beta = 0.36$. Inset: data for α-relaxation for all temperatures measured.

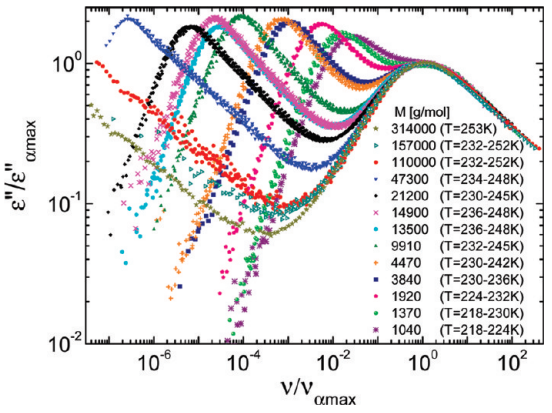

Figure 5. Molecular weight dependence of the dielectric spectra (high-temperature data as indicated) of the different polyisoprenes investigated; dielectric permittivity ε'' rescaled by its α-peak height $\varepsilon''_{\alpha\mathrm{max}}$ displayed as a function of frequency ν rescaled by the α-peak frequency $\nu_{\alpha\mathrm{max}}$.

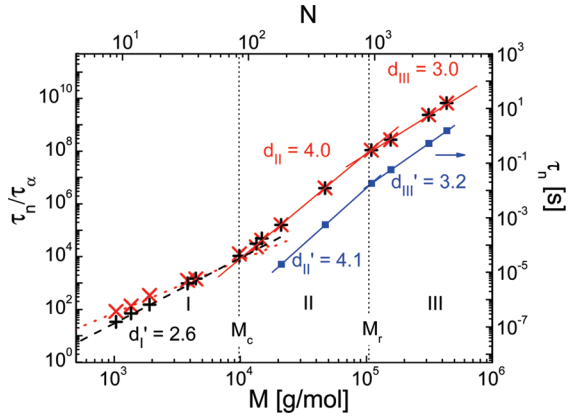

Figure 6. Ratio τ_n/τ_α of normal mode τ_n and α-relaxation time τ_α as a function of molecular weight M (lower scale) and of number of subchains $N = M/M_R$ (upper scale): black plus: $\tau_n/\tau_\alpha = \nu_{\alpha\mathrm{max}}/\nu_{\mathrm{nmax}}$ obtained from Figure 5; dashed line (regime I): power-law fit with exponent d_I'; red solid lines (regimes II and III): with exponent d_{II} and d_{III}, respectively; red crosses: τ_n/τ_α taken from separating normal mode and α-relaxation (cf. Figure 10a); red dotted line (regime I): interpolation by eq 7 and taking $M_R = 110$; blue squares: $\tau_n = 1/(2\pi\nu_{\mathrm{nmax}})$; blue lines: power-law fits for $\tau_n(M)$ at $T = 350$ K with exponents d' as indicated.

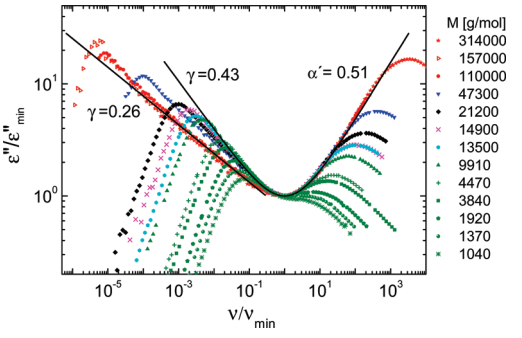

Figure 7. Relaxation minimum observed in Figure 5 rescaled by its position ν_{min} and height $\varepsilon''_{\mathrm{min}}$. Solid lines mark power-law flanks with exponents as indicated.

laws with M independent exponents. The high-frequency flank of the normal mode relaxation is described by an exponent $\gamma = 0.43$. At $M > 9910$ this exponent decreases continuously until it reaches saturation at highest M, yielding another power-law flank with $\gamma = 0.26$ (data marked red). Given the fact that $M = 9910 \cong M_c$, we attribute the M independent flank of the normal mode relaxation to the Rouse regime, whereas at higher M the spectra change with M due to the onset of entanglement effects. Regarding the α-relaxation, for all M the exponent $\alpha' = 0.51$ of its low-frequency flank virtually does not change. We once again conclude that at high temperatures the spectral shape of the α-relaxation is M as well as T independent.

Whereas the data representation in Figure 7 focuses on the shape of the high-frequency flank of the normal mode relaxation as well as the α-process, in Figure 8 we show the data $\varepsilon''(\nu)/\varepsilon''_{\mathrm{nmax}}$ versus ν/ν_{nmax} which allows inspecting the low-frequency part of the normal mode relaxation. At $\nu \leq \nu_{\mathrm{nmax}}$ the data agree well, and the low-frequency flank is described by a Debye behavior, i.e., $\varepsilon(\nu) \propto \nu^1$, as expected for the terminal relaxation. In other words, the low-frequency part of the normal mode relaxation is M independent, which we take as an indication that the molecular weight

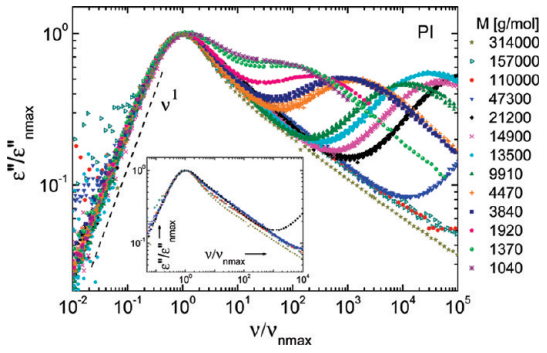

Figure 8. Molecular weight dependence of the dielectric spectra of the different polyisoprenes investigated: dielectric permittivity ε'' rescaled by its normal mode peak height $\varepsilon''_{\mathrm{nmax}}$ displayed as a function of frequency ν rescaled by the normal mode peak frequency ν_{nmax}. Inset: data in the limit of high M.

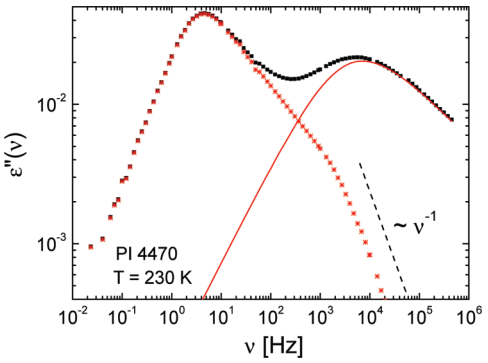

Figure 9. Typical spectral decomposition of normal mode and α-relaxation spectrum: black, experimental data; red solid line, interpolation of the α-peak by a HN function. The normal mode spectrum (red stars) exhibits a high-frequency cutoff showing a Debye behavior $\varepsilon''(\omega) \propto \nu^{-1}$ (dashed line).

polydispersity, which actually increases somewhat for lowest M, does not play a role. The scatter at lowest frequencies observed for high M is due to the subtraction of the dc contribution. In the inset of Figure 8 one can recognize that, in addition to the decrease of the high-frequency exponent γ, the onset of the high-frequency wing occurs at higher frequencies and lower amplitudes the higher M.

To further analyze the spectral shape of the normal mode relaxation, we subtracted the contribution of the α-process from all the dielectric spectra by assuming an M and T independent spectral shape of the α-peak. The corresponding shape parameters were obtained by interpolating the spectra of the α-process for the high-M samples by a HN function[38] (cf. Figures 4c and 19). In this case, only a weak overlap of the spectral contributions of normal mode and α-relaxation is present. As the best fit, we find the parameters $\alpha = 0.70$ and $\beta = 0.36$. Here two notes are worthwhile. (i) Comparing the low-frequency exponent of the α-relaxation, $\alpha = 0.70$, with the corresponding exponent $\alpha' = 0.51$ of the "minimum scaling" (cf. Figure 7), a significant difference is found. By determining the exponent α' from the minimum scaling, we assumed that the high-frequency flank of the normal mode spectrum with exponent $\gamma = 0.43$ continues to extend to frequencies covered by the α-relaxation. However, this is not expected as the normal mode spectrum has to show a cutoff close to $\tau_s = \tau_\alpha$. For example, in the Rouse theory the spectrum turns over to a Debye behavior following a ω^{-1} law at $\omega\tau_s \cong 1$ (cf. Figure 1). As $\alpha' < \alpha$ we conclude that the cutoff is already present at $\omega\tau_\alpha = \nu/\nu_{\mathrm{max}} \leq 1$ and moreover that the cutoff is characterized by a power law with an exponent larger than $\gamma = 0.43$. In other words, we expect to see the cutoff when subtracting the spectral contribution of the α-relaxation. Indeed, this is what is found (cf. below, e.g., Figure 10). (ii) An exponent α characterizing the low-frequency flank of the α-relaxation being lower than 1 ($\alpha = 0.70$) is unphysical in the sense that it does not reflect the correct low-frequency limit of a reorientational correlation function. In the case of low-molecular-weight glass-formers as well as type B polymers usually a Debye limit, i.e., $\alpha = 1$, is observed provided that sufficiently low frequencies are studied.[9,49] However, the present spectra of PI can only be interpolated by $\alpha < 1$. Introducing a low-frequency Debye cutoff at very low frequencies and very low intensity will not significantly alter the result of the subtraction procedure. Here we note that the phenomenological validity of the HN susceptibility may be an indication of the influence of the cross-relaxation effects mentioned in the Theoretical Background section.

For the subtraction procedure, given the width parameters α and β, we have to find a criterion to fix the amplitude and time constant of the α-relaxation. Depending on the criteria, the cutoff of the normal mode spectrum will manifest itself in different ways. Here, we assumed that the cutoff of the normal relaxation is supposed to be Debye-like as predicted by the Rouse theory (cf. Figure 1a), and we chose amplitude and time constant $\tau_\alpha = 1/(2\pi\nu_{\alpha\mathrm{max}})$ of the α-relaxation accordingly. We will come back to this point in the Discussion part. A typical spectral decomposition is shown in Figure 9. In addition, we normalized the normal mode spectra such that their integral is $\pi/2$ and rescaled the frequency axis by $\tau_\alpha = 1/(2\pi\nu_{\alpha\mathrm{max}})$ (see Figure 10a). The ratio τ_n/τ_α as obtained from the decomposed spectra is included in Figure 6 (red crosses). As expected differences occur at low M with respect to the data obtained by "peak picking" of the spectra in Figure 5, and the apparent exponent in the Rouse regime decreases somewhat to $d_1 = 2.2$. Still, the discrete Rouse model (cf. eq 7) which actually does not yield a power-law M dependence also well interpolates the data at $M \leq 4470$ (red solid line in Figure 6) provided that the molecular weight of the Rouse unit is taken as $M_R = M/N = 110$.

In Figure 10a the so-obtained normal mode spectra are displayed. At high frequencies a cutoff located close to $\omega\tau_\alpha = \nu/\nu_{\alpha\mathrm{max}} = 1$ is recognized, which signals the end of the polymer spectra. For the four PI samples with highest M we show the original spectra as the frequency range of the α-peak is not covered together with the normal mode peak. Once again, the power-law behavior in the range $\nu/\nu_{\mathrm{nmax}} \ll \nu/\nu_{\alpha\mathrm{max}} \ll 1$ is well seen, and the corresponding exponent γ decreases with M at $M > 9910$. Regarding the data for $M < 9910$, the prediction of the discrete Rouse theory is shown in Figure 10b. We emphasize that both the experimental spectra and the theoretical spectra are normalized to the same integral ($\pi/2$); i.e., experiment and theory are compared on absolute scale. Though the Rouse theory captures the essential features of the spectra, systematic deviations are recognized. The normal mode spectra are broader than predicted, a fact well-known from previous studies.[11,32,34]

As demonstrated in the Theoretical Background section (cf. Figure 1), following the Rouse model the normal mode spectra can be shifted vertically to yield a universal envelope at $\nu/\nu_{\mathrm{nmax}} \ll \nu/\nu_{\alpha\mathrm{max}} \ll 1$. In Figure 11a,b, this scaling is applied for the experimental spectra of Figure 10a by employing a suitable shift factor SF. As reference the spectrum for $M = 4470$ is used. For the samples with $M \leq 9910$ (marked green in Figure 11a), indeed, a power-law envelope is found with an exponent $\gamma = 0.43 \pm 0.03$, which is somewhat

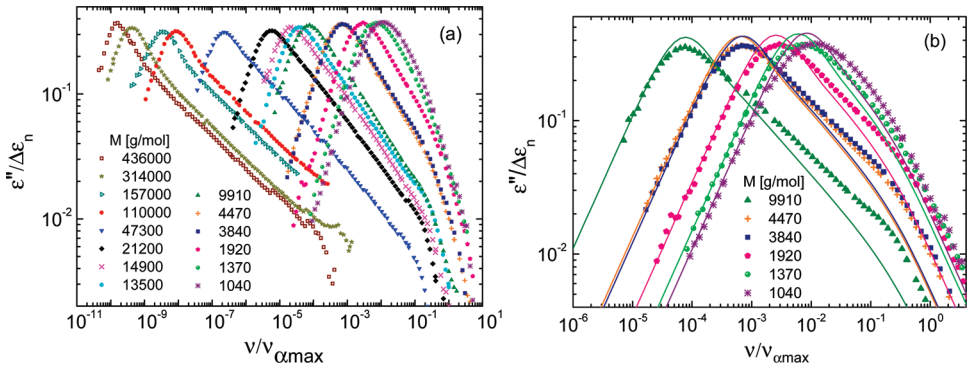

Figure 10. (a) Normalized normal mode spectra of all samples as a function of reduced frequency $\nu/\nu_{\alpha max}$ obtained after subtracting the α-relaxation ($M \leq 47\,300$) from the overall spectra, note high-frequency cutoff; for $M > 47\,300$ spectra without subtraction of α-relaxation are shown. (b) Data as in (a) but for $M \leq 9910$ only. Solid lines: predictions by the Rouse theory.

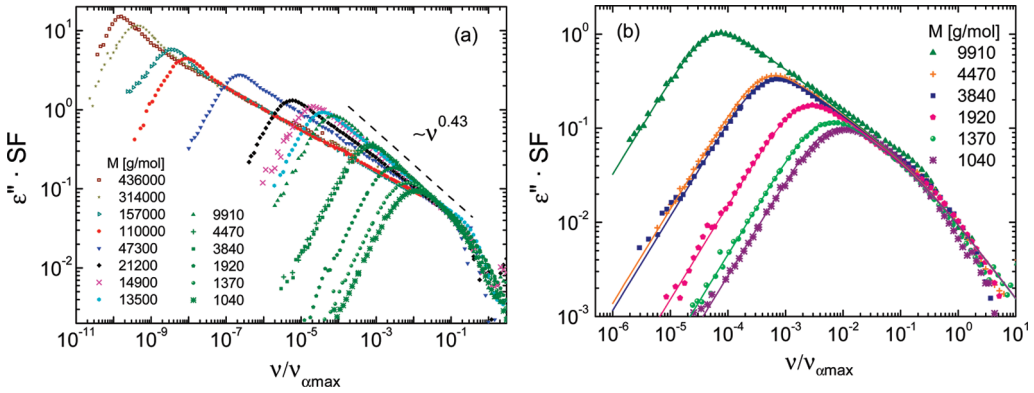

Figure 11. (a) Normal mode spectra shifted (SF) to yield a common envelope; at $M > 9910$ spectra are shifted to agree at the high-frequency cutoff; green data points mark Rouse regime; dashed line: power-law envelope with exponent as indicated. (b) Same spectra as in (a) for $M \leq 9910$ only; solid-lines: prediction by the modified Rouse theory with stretched exponential ($\beta_K = 0.8$) correlation function for each mode.

lower than that expected from Rouse theory ($\gamma_{Rouse} = 0.5$). For the other spectra with $M > 9910$ no common envelope is observed, and the spectra are shifted to coincide with the high-frequency cutoff of the spectra at $M \leq 9910$; here, as said, entanglement effects become relevant. However, for the four highest M values, the high-frequency flank of the normal spectra exhibits the same power-law behavior, again suggesting that saturation occurs, and another characteristic envelope with $\gamma = 0.26 \pm 0.01$ is observed. Important to note, even at highest frequencies the behavior of these normal mode spectra does not agree with that in the Rouse regime; i.e., the Rouse theory is not able to describe the dynamics at short times in the entanglement regime, in contrast to what is often assumed.[2,3,29]

It is well-known from computer simulations that the Rouse modes are actually not described by an exponential decay but rather by some stretched exponential decay.[20−23,25] Thus, we show in Figure 11b the interpolation of the rescaled spectra by assuming a stretching parameter of $\beta_K = 0.8$ for all modes (cf. eq 16). This provides a significant improvement of interpolating the experimental spectra. As the stretching of the normal modes is quite moderate, also the high-frequency cutoff is fairly well interpolated. The approach could even be improved by introducing a stretching being mode dependent, i.e., $\beta_K = \beta_K(p)$. We conclude that the Rouse model allows for a virtually perfect interpolation of the spectra at $M < M_c$ provided that we allow for a moderate stretching of the correlation function of each individual normal mode.

In order to obtain the spectra in Figure 11, a shift factor (SF) was applied which can be compared to that of the theory, i.e., to $\langle R^2(0)\rangle/b^2$ (cf. Theoretical Background section). As seen in Figure 12, SF essentially follows that expected by the discrete Rouse model assuming a stretching parameter of $\beta_K = 0.8$. Actually, in the M range studied the discrete and continuous Rouse model do not differ, and again we find $M_R = 110$. For comparison, we included the behavior for the standard discrete Rouse model ($\beta_K = 1$) which provides an inferior interpolation. At $M > 9910$ a different trend is observed for SF which is attributed to the dominance of entanglement effects.

In the entanglement regime ($M > 9910$), as said, the exponent γ of the high-frequency flank decreases with M. This is seen in Figure 13. Starting from an essentially constant value of $\gamma = 0.43$ in the Rouse regime at $M \leq 10^4$, the exponent continuously drops until it saturates around $M = 10^5$, yielding an exponent $\gamma = 0.26$. Important to note is that the saturation of these spectral changes is reached when the power-law exponent d turns back from $d_{II} = 4.0$ to $d_{III} = 3.0$ (cf. Figure 6).

Finally, we show in Figure 14 the ratio $\Delta\varepsilon_n/\Delta\varepsilon_\alpha$ of the relaxation strength of the normal mode and α-relaxation spectrum. An increase is observed at low M and saturation is reached essentially at $M > 2000$. As mentioned before, two data points (brackets) do not fit into the overall trend. Yet, after normalization the corresponding spectral shape follows the trend (cf. Figure 11a). We note that $\Delta\varepsilon_n/\Delta\varepsilon_\alpha$ is expected to become M independent when Gaussian statistics are established (cf. Theoretical Background section). Given the data in Figure 14, we conclude that this occurs well below $M_e = M_c/2$. Similar results were reported by Imanishi et al. for PI[32] and by Gainaru et al.[50] for poly(propylene oxide); however, they appear to be in contrast to findings from

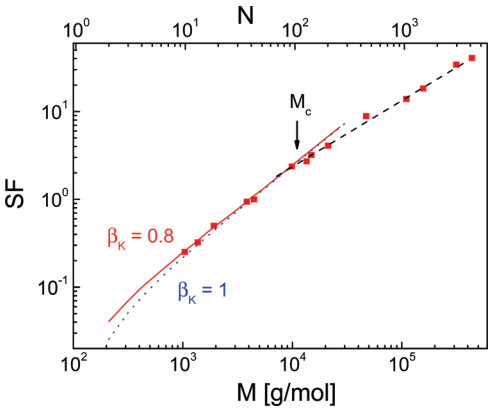

Figure 12. Shift factor (SF) as a function of molecular weight M yielding the master curves in Figure 11b, reference system is PI 4470: dotted blue line: standard discrete Rouse theory; solid red line: discrete Rouse theory with correlation functions stretched as indicated; dashed line: guide for the eye for data at $M > 9910 \cong M_c$; upper axis refers to number $N = M/M_R$ of Rouse subchains with $M_R = 110$.

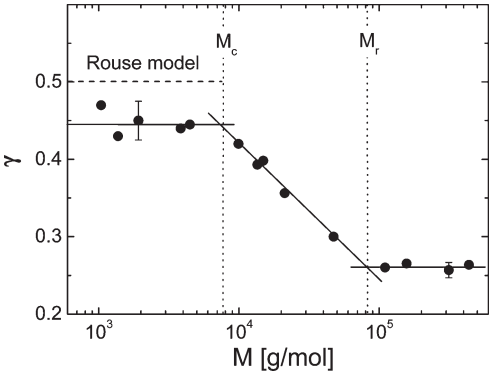

Figure 13. Exponent γ of the high-frequency power law of the normal mode spectra shown in Figure 10a as a function of M; solid lines: guide for the eye; dashed line: expectation from Rouse theory; characteristic molecular weights $M_c \cong 2M_e$ and M_r indicated.

neutron scattering where the crossover to Gaussian statistics is observed at much higher M.[51]

Relaxation Times. Parts a and b of Figure 15 display the time constants of the segmental or α-process τ_α and the normal mode time constant τ_n, respectively, as a function of temperature obtained from the peak frequencies via $\tau = 1/(2\pi\nu_{max})$. We note that in the Rouse regime the relaxation time τ_n is essentially identical with the Rouse time τ_R.[3,29] In Figure 15a we included the results from our FFC NMR study.[52] Together, DS and NMR cover relaxation times extending over more than 11 decades, and each joint data set can be fully interpolated by a single Vogel−Fulcher−Tammann (VFT) equation. Defining the glass transition temperature T_g through $\tau_\alpha(T_g) \equiv 1$ s, its M dependence is shown in the inset of Figure 15a. A continuous increase of $T_g(M)$ is observed until saturation occurs at high M; the data are interpolated by the Fox−Flory equation.[53] In contrast to recent results for several other polymers,[49] no discontinuous dependence on M is recognized.

In a recent publication, Abou Elfadl et al.[54] demonstrated that in the case of a series of a given polymer with different M the temperature dependence of the relaxation time is best reproduced by a function $f(T - T_g)$. Thus, a master curve results when all data $\tau(T)$ are shifted by T_g. This is done in Figure 16a for τ_α and in Figure 16b for τ_n. In the latter case, shifting the data sets in a second step vertically (parameter A)

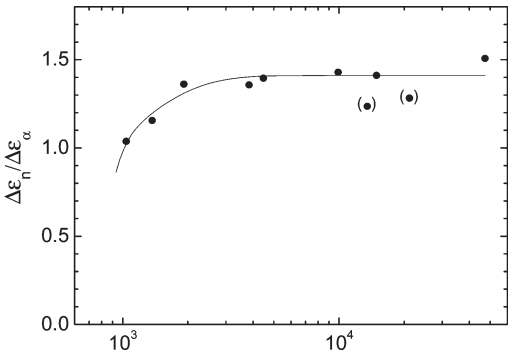

Figure 14. Ratio $\Delta\varepsilon_n/\Delta\varepsilon_\alpha$ of the relaxation strength of normal mode and α-relaxation as a function of M; solid line: guide for the eye; two data points (brackets) do not fit in the overall trend.

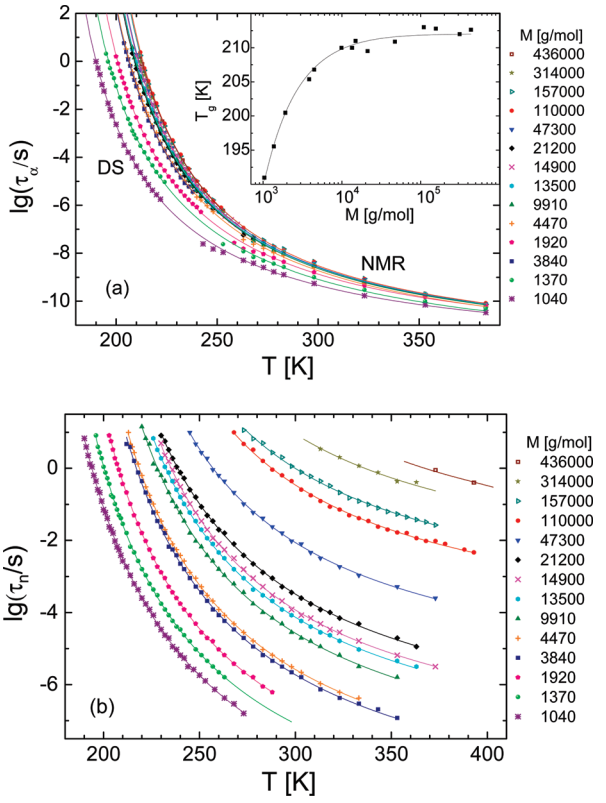

Figure 15. (a) Segmental correlation time, $\tau_\alpha = 1/(2\pi\nu_{\alpha max})$, as a function of temperature; in addition, we included the results from field cycling NMR.[52] Inset: glass transition temperature T_g (defined as $\tau(T_g) \equiv 1$ s) as a function of molecular weight M, interpolation by Fox−Flory equation.[53] (b) Normal mode correlation time, $\tau_n = 1/(2\pi\nu_{nmax})$, as a function of temperature. In both figures, solid lines represent fits by the Vogel−Fulcher−Tammann equation.

provides a master curve for all M. In terms of the parameters of the VFT equation, namely D and T_0, this kind of scaling works if D is constant and only T_0 is changing but under the condition that $T_g - T_0 =$ constant. In other words, for a given polymer system the quantity F

$$F = -\left.\frac{\mathrm{d}\log\tau_\alpha}{\mathrm{d}T}\right|_{T_g} = \frac{D}{(T_g - T_0)^2} = m/T_g \qquad (18)$$

is a constant independent of M, and fragility m is just proportional to T_g as $m = FT_g$ holds.[49,54] We note that deviations from the master curve occur in the limit of the

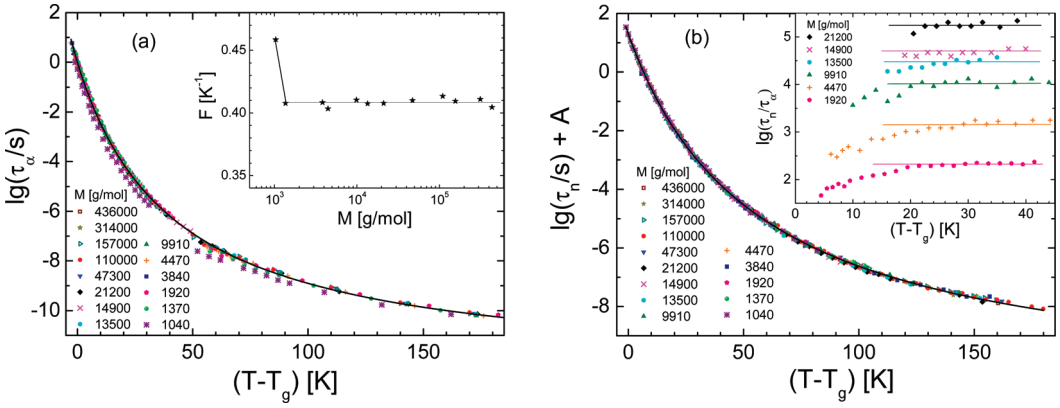

Figure 16. (a) Master curves for the time constant (τ_α) of α-relaxation. (b) Normal mode relaxation τ_n applying a parameter A to collapse data for different M, temperature scale shifted by glass transition temperature T_g. Inset in (a): parameter $F(M)$ (cf. eq 18) adjusted to the definition $\tau_\alpha(T_g) = 100$ s; solid line: guide for the eye. In (b): ratio τ_n/τ_α as a function of $T - T_g$; solid-line: guide for the eye.

nonpolymeric or simple liquid regime, e.g., at $M = 1040$ in the case of PI as recognized in Figure 16a; cf. also inset showing $F(M)$.

As emphasized also by others,[33,35,55] the temperature dependences of τ_α and τ_n slightly differ. Fitting the data with a VFT equation, we find $D = 518.3\ K^{-1}$ and $T_g - T_0 = 41.2$ K for the segmental dynamics and $D = 690.9\ K^{-1}$ and $T_g - T_0 = 55.8$ K for the normal mode (cf. solid lines in Figure 16). A direct comparison is possible when $\tau_n(T)/\tau_\alpha(T)$ is plotted (cf. inset Figure 16b). Clearly, at high temperatures FTS applies for the overall spectra whereas at low temperatures close to T_g some decoupling is observed (cf. also Figure 4a). Full FTS being applicable at high temperatures was also reported by other authors.[33,35,36,55] We emphasize that the decoupling at low temperatures is rather small as the ratio changes by a factor less than 10.

V. Discussion and Conclusions

Sixteen PI samples were measured covering a wide range of molecular weights with M varying from 652 to 4.36×10^5. This corresponds to a maximum $Z = M/M_e \cong 87$, which is more than was investigated in most other studies before. An important result of our analysis is that we can reproduce quantitatively the normal mode spectra in the Rouse regime ($1040 \le M \le 9910$) provided that we phenomenologically introduce a weak stretching ($\beta_K = 0.8$) of the correlation function of the individual modes. This takes into account the somewhat broader spectra as compared to the standard Rouse theory. The broadening is well-known from other works,[29,11,32,34,21] but it does apparently not change in the Rouse regime. Consequently, after appropriately rescaling the spectra, a master curve is found which displays a power-law envelope with an exponent $\gamma = 0.43 \pm 0.03$, which is somewhat below the expectation of the standard Rouse model ($\gamma_{Rouse} = 0.5$) (cf. Figures 11b and 13). The possibility to construct a master curve allows distinguishing the Rouse regime from the entanglement regime ($M > 9910$). Given this master curve as well as the collapse of the normal mode relaxation peak at $\nu/\nu_{nmax} \le 1$ (cf. Figure 8), we do not think that in the present study polydispersity of the molecular weight hampers the analysis (cf. Table 1).[29,32] We also emphasize that the finding of an M independent envelope of the dielectric spectra in the Rouse regime does not rely on subtracting the α-peak; it is already identified, e.g., through the minimum scaling (cf. Figure 7).

At M above the crossover molecular weight $M_c \cong 2M_e \cong 10^4$ the normal mode spectra change their shape; in particular, the exponent of the high-frequency power law decreases until it reaches a value of $\gamma = 0.26 \pm 0.01$ around $M = 10^5$. Imanishi et al.,[32] also subtracting the α-process contribution, found a similar broadening with M whereas Watanabe[3,29] reported that the normal mode distribution is essentially independent of M, when the raw data are inspected. Once again, polydispersity is not expected to cause these results,[29] and our results regarding $\gamma(M)$ do not depend on whether the α-relaxation is subtracted or not since at high M the spectral overlap is irrelevant. Finally, we note that the crossover from $\gamma = 0.43$ (Rouse regime) to $\gamma = 0.26$ in the high M limit is very similar to what has been observed for PI probes in PB matrices as well as for PI in solution when increasing the concentration.[3,29]

As discussed above, within the tube-reptation model free Rouse dynamics are predicted at $\tau_\alpha < t < \tau_e$.[2,3,29] In other words, the high-frequency behavior of the polymer dynamics are expected to be the same as for $M < M_e$ what is also found in FFC NMR.[18,56] However, this is not observed in the dielectric spectra, and the exponent $\gamma = 0.26$ found at highest M is actually not expected for pure tube reptation. Combining reptation and contour length fluctuations predicts $\gamma = 0.25$.[57] As discussed by Watanabe,[29] this combined model, however, does not consistently describe the viscoelastic behavior of PI.

Coinciding with the saturation of the high-frequency exponent $\gamma(M)$ of the normal mode spectrum at $M > 10^5$, we observe that the exponent d of the M dependence of the ratio τ_n/τ_α returns from $d_{II} = 4.0 \pm 0.2$ back to $d_{II} = 3.0 \pm 0.2$. In other words, above $M = 10^5$ the exponent of pure tube-reptation dynamics is observed.[2] Concerning DS, such a result was not reported before probably because most of the studies focused on rather moderate M values. Actually obtaining the ratio τ_n/τ_α for high M values was possible because we relied on the master curve $\tau_\alpha = f(T - T_g)$ extending to very high temperature by including NMR data (cf. Figure 16a). Of course, at highest M the change of τ_α with M is negligible for a given temperature. In other words, displaying just $\tau_n(M)$ is expected to yield the same result, and this is also found (cf. Figure 6, solid squares and corresponding exponents d'). An exponent of $d_{II}' = 3.2$ is observed. We also stress that the ratio τ_n/τ_α is temperature independent only above say $T = T_g \pm 35$ K, and only at such temperatures its M dependence can be analyzed.

It is well-known that the pure tube-reptation model with fixed tube constraints imposed by surrounding chains does not fully account for the experimental findings at $M > M_c$. For example, the terminal relaxation time τ_t does not follow a power law $\tau_t \propto M^3$ but rather $\tau_t \propto M^{3.4-3.7}$;[3,5,29] this is once again confirmed by our experiments although we find a somewhat higher exponent of $d_{II} = 4.0$ when restricting the interpolation to the range $10^4 < M < 10^5$ (cf. Figure 6). Several models were developed to incorporate topological fluctuations such as contour length fluctuations or constraint release.[2−6,29] However, there are some indications (and speculations) that finally at very high M true

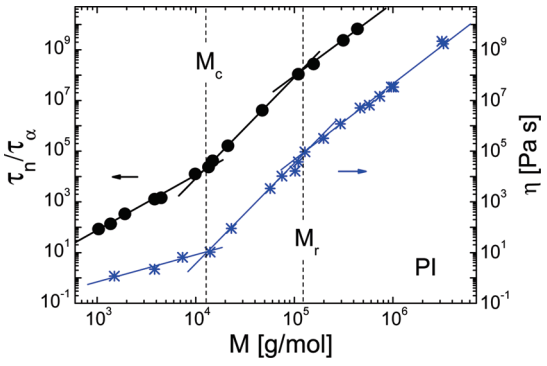

Figure 17. Ratio τ_n/τ_α of normal mode τ_n and α-relaxation time τ_α as a function of molecular weight M (solid circles, data from Figure 6) compared to the behavior of the viscosity (stars, taken from ref 58). Straight solid lines: guide for the eye; dashed lines mark characteristic molecular weights M_e and M_r.

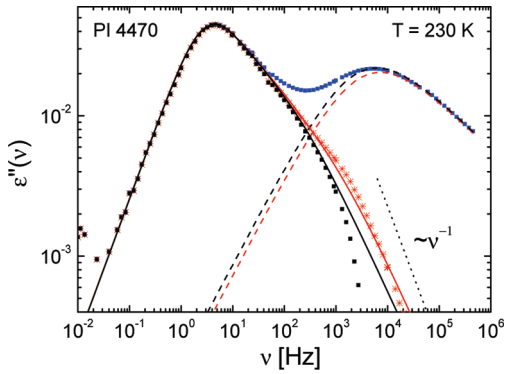

Figure 18. Normal mode spectrum for polyisoprene (PI) as obtained by different ways to account for the α-relaxation (dashed curves). Red stars: assuming that the cutoff exhibits a Debye behavior, $\varepsilon'' \propto \nu^{-1}$ (dotted line); black squares: assuming that for $\omega\tau_\alpha > 1$ the contribution of the normal mode relaxation can be ignored; solid lines: interpolation with the modified Rouse model with $N = 38$ and 18, respectively.

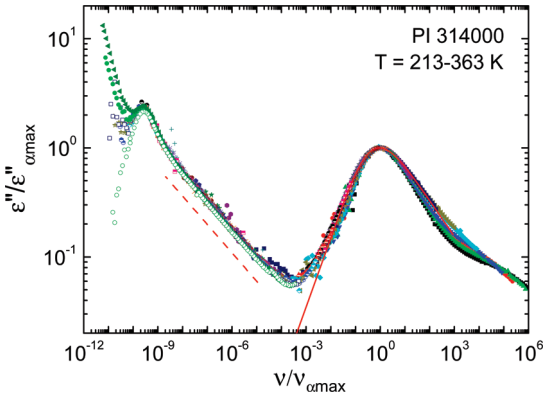

Figure 19. Dielectric spectrum obtained from data of a temperature range as indicated rescaling amplitude and frequency axis by $\varepsilon_{\alpha max}$ and $\nu_{\alpha max}$, respectively. Open green circles: one spectrum after subtraction of the dc contribution; red solid line: interpolation of the α-relaxation by a HN function with exponents $\alpha = 0.7$ and $\beta = 0.36$ (cf. Figure 4c); dashed line: power law $\nu^{-\gamma}$ with $\gamma = 0.26$.

tube reptation may establish.[5,6] In the case of PI, Abdel-Goad et al.[58] reported that at M larger than, say, 2×10^5 the viscosity exponent turns back to 3.1, whereas it is 3.9 in the range $1.3 \times 10^4 < M < 2 \times 10^5$. In Figure 17 we show a comparison of the viscosity data of Abdel-Goad et al. with our results after subtracting the contribution of the α-process. Indeed, very similar exponents and crossover molecular weights are recognized ($M > M_e$). Note that the viscosity exponent in the Rouse regime is expected to be 1 as also reported by the authors. We also note that the PI samples of Abdel-Goad et al. were purchased from the same supplier (PSS). Given this good agreement with our results, we conclude that in addition to M_e or M_c a further characteristic molecular weight, namely M_r, has to be introduced, beyond which the exponent typical of pure tube reptation is reached and the high-frequency exponent γ saturates. In agreement with simulation[20] as well as NMR studies,[18,56,59] the crossover from Rouse dynamics to fully established entanglement dynamics is highly protracted occurring only beyond, say, $M_r = 20M_e \cong 10^5$ for PI. It appears that an exponent $\gamma \cong 0.26 \pm 0.01$ of the high-frequency flank of the normal mode spectrum is characteristic of this regime.

There is an important problem to be addressed regarding the molecular weight of the Rouse subchain or the Rouse unit M_R. On the one hand, from analyzing the ratio τ_n/τ_α as a function of M, we obtain $M_R \cong 110$ (cf. Figure 6 and also Figure 12). On the other hand, inspecting the dielectric spectra of the low-M systems PI 790 and PI 690, we do not find clear indications of a normal mode relaxation. Our ongoing FFC NMR study of PI reveals no sign of polymer dynamics for $M < 1000$ either.[52] Well-established normal mode spectra are dielectrically first observed at $M \cong 1040$; i.e., at least two Rouse beads have to be involved in this case. Then, we can estimate $M_R \cong 520$. Adachi et al. reported $M_R = 630$ for PI,[60] and in the case of PB we found $M_R \cong 500$ applying FFC NMR.[17] The two estimates, i.e., $M_R \cong 110$ and $M_R \cong 520$, differ significantly. The width of the Rouse spectrum is fixed by the Rouse time τ_R on the low-frequency side and by the cutoff time $\tau_{cut} \cong \tau_s \cong \tau_\alpha$ on the high-frequency side. In this case, the "knee" indicating the crossover to the cutoff appears at $\omega\tau_\alpha \cong \nu/\nu_{\alpha max} \cong 0.2$ (cf. Figure 1a). Approximately, this is also found in our analysis (cf. Figure 11). However, the position of the cutoff depends on the way the α-relaxation peak is subtracted. This is demonstrated in Figure 18 where we show two normal mode spectra obtained with different criteria for subtracting the α-peak. In the first case (red stars) we assumed as above that the cutoff has to be Debye-like, whereas in the second case (black squares) we assumed that the spectral contribution of the normal mode relaxation may be ignored at $\nu/\nu_\alpha > 1$. Clearly, the cutoff times differ by a factor of 2−3; nonetheless, the exponent γ of the high-frequency flank is virtually not altered. A factor of 3 would directly lead to $M_R \cong 330$. We did not recourse to the second procedure as in this case the shape of the cutoff becomes Gaussian-like which is actually unphysical. Of course, our first estimate depends on identifying M_R under the condition $\tau_n = \tau_\alpha$, a procedure which could be challenged. Concluding the problem of identifying the Rouse subchain is still unsolved. More DS data on low-M systems with well-defined microstructure and low polydispersity are needed.

Acknowledgment. We thank Anja Goldmann, Sabine Wunder (Makromolekulare Chemie II, Universität Bayreuth), and Christina Löffler (Makromolekulare Chemie I, Universität Bayreuth) for GPC measurements. The authors appreciate financial support by the Deutsche Forschungsgemeinschaft (DFG) through SFB 481 and RO 907/13. A. Abou Elfadl is grateful for her Egyptian State Fellowship.

Appendix

Figure 19 shows a combined dielectric spectrum for PI 314000 extending over 17 decades in frequency obtained from data at different temperatures by rescaling the amplitude and frequency axis with $\varepsilon_{\alpha max}$ and $\nu_{\alpha max}$, respectively. Although the separation of normal mode and α-relaxation is too large for allowing to test FTS for the full response, the latter is fulfilled for each normal mode and α-relaxation individually. At lowest frequencies

contributions from the dc conductivity are recognized which were accounted for by subtracting the corresponding power law. Then, a well-resolved normal mode relaxation peak is recognized (open green circles). Actually, the dc contribution limits the analysis at high M. Regarding the α-peak, at high frequencies traces of a secondary relaxation are discernible which do not follow FTS.

References and Notes

(1) De Gennes, P. G. *J. Chem. Phys.* **1971**, *55*, 572–579.
(2) Doi, M.; Edwards, S. F. *The Theory of Polymer Dynamics*; Oxford Science Publications: Oxford, 1986.
(3) Watanabe, H. *Prog. Polym. Sci.* **1999**, *24*, 1253–1403.
(4) McLeish, T. C. B. *Adv. Phys.* **2002**, *51*, 1379–1527.
(5) Dealy, J. M.; Larson, R. G. *Structure and Rheology of Molten Polymers*; Hanser Publications: Munich, 2006.
(6) Leeuwen, J. M. J.; Drzewinski, A. *Phys. Rep.* **2009**, *475*, 53–90.
(7) Angell, C. A.; Ngai, K. L.; McKenna, G. B.; McMillan, P. F.; Martin, S. W. *J. Appl. Phys.* **2000**, *88*, 3113–3157.
(8) Lunkenheimer, P.; Schneider, U.; Brand, R.; Loidl, A. *Contemp. Phys.* **2000**, *41*, 15–36.
(9) Blochowicz, T.; Brodin, A.; Rössler, E. A. *Adv. Chem. Phys.* **2006**, *133* (Part A), 127−256.
(10) Stockmayer, W. H. *Pure Appl. Chem.* **1967**, *15*, 539–554.
(11) Plazek, D. J.; O'Rourke, V. M. *J. Polym. Sci.* **1971**, *9* (Part A-2), 209−243.
(12) Adachi, K.; Kotaka, T. *Macromolecules* **1985**, *18*, 466–472.
(13) Adachi, K.; Kotaka, T. *Macromolecules* **1988**, *21*, 157–164.
(14) Fetters, L. J.; Lohse, D. J.; Richter, D.; Witten, T. A.; Zirkel, A. *Macromolecules* **1994**, *27*, 4639–4647.
(15) Richter, D.; Monkenbusch, M.; Arbe, A.; Colmenero, J. *Neutron Spin Echo in Polymer Systems*; Springer: Berlin, 2005.
(16) Kimmich, R.; Anoardo, E. *Prog. NMR Spectrosc.* **2004**, *44*, 257–320.
(17) Kariyo, S.; Brodin, A.; Gainaru, C.; Herrmann, A.; Hintermeyer, J.; Schick, H.; Novikov, V. N.; Rössler, E. A. *Macromolecules* **2008**, *41*, 5322–5332.
(18) Herrmann, A.; Novikov, V. N.; Rössler, E. A. *Macromolecules* **2009**, *42*, 2063–2068.
(19) Binder, K.; Paul, W. *J. Polym. Sci., Part B: Polym. Phys.* **1997**, *35*, 1–31.
(20) Kreer, T.; Baschnagel, J.; Müller, M.; Binder, K. *Macromolecules* **2001**, *34*, 1105–1117.
(21) Doxastakis, M.; Theodorou, D. N.; Fytas, G.; Kremer, F.; Faller, R.; Müller-Plathe, F.; Hadjichristidis, N. *J. Chem. Phys.* **2003**, *119*, 6883–6894.
(22) Smith, G. D.; Borodin, O. J.; Paul, W. *Chem. Phys.* **2002**, *117*, 10350–10359.
(23) Padding, J. T.; Briels, W. J. *J. Chem. Phys.* **2002**, *117*, 925–943.
(24) Binder, K.; Baschnagel, J.; Paul, W. *Prog. Polym. Sci.* **2003**, *28*, 115–172.
(25) Paul, W.; Smith, G. D. *Rep. Prog. Phys.* **2004**, *67*, 1117–1185.
(26) Smith, G. D.; Bedrov, D. *J. Polym. Sci., Part B* **2007**, *45*, 627–643.
(27) Boyd, R. H.; Smith, G. D. *Polymer Dynamics and Relaxation*: Cambridge University Press: New York, 2007.
(28) McCrum, N. G.; Read, B. E.; Williams, G. *Anelastic and Dielectric Effects in Polymer Solids*; Dover Publications: New York, 1991.
(29) Watanabe, H. *Macromol. Rapid Commun.* **2001**, *22*, 127–175.
(30) Kremer, F., Schönhals; A., Eds.; *Broadband Dielectric Spectroscopy*; Springer: Berlin, 2003.
(31) Riande, E.; Diaz-Calleja, R. *Electric Properties of Polymers*; Marcel Dekker: New York, 2004.
(32) Imanishi, Y.; Adachi, K.; Kotaka, T. *J. Chem. Phys.* **1988**, *89*, 7585–7592.
(33) Adachi, K.; Hirano, H. *Macromolecules* **1998**, *31*, 3958–3962.
(34) Boese, D.; Kremer, F. *Macromolecules* **1990**, *23*, 829–835.
(35) Schönhals, A.; Schlosser, E. *Phys. Scr.* **1993**, *T 49*, 233–236.
(36) Schönhals, A. *Macromolecules* **1993**, *26*, 1309–1312.
(37) Ferry, J. D. *Viscoelastic Properties of Polymers*, 3rd ed.; Wiley: New York, 1980.
(38) Williams, G. *Chem. Rev.* **1972**, *72*, 55–69.
(39) Böttcher, C. J. F.; Borderwijk, P. *Theory of Electric Polarization*, 2nd compl. rev. ed.; Elsevier: Amsterdam, 1978; Vol. *2*.
(40) Havriliak, S.; Negami, S. *J. Polym. Sci., Part C* **1966**, *14*, 99–117.
(41) Rouse, P. E. *J. Chem. Phys.* **1953**, *21*, 1272–1280.
(42) Verdier, P. H. *J. Chem. Phys.* **1966**, *45*, 2118–2121.
(43) Rubinstein, M.; Colby, R. H. *Polymer Physics*; University Press: Oxford, 2005.
(44) Wagner, H.; Richert, R. *J. Phys. Chem. B* **1999**, *103*, 4071–4077.
(45) Brodin, A.; Gainaru, C.; Porokhonskyy, V.; Rössler, E. A. *J. Phys.: Condens. Matter* **2007**, *19*, 205104–1−14.
(46) Williams, G. *Adv. Polym. Sci.* **1979**, *33*, 59–92.
(47) Goldstein, J. *J. Chem. Phys.* **1970**, *53*, 2372–2388.
(48) Kudlik, A.; Benkhof, S.; Tschirwitz, C.; Blochowicz, T.; Rössler, E. *J. Mol. Struct.* **1999**, *479*, 201.
(49) Hintermeyer, J.; Herrmann, A.; Kahlau, R.; Goiceanu, C.; Rössler, E. A. *Macromolecules* **2008**, *41*, 9335–9344.
(50) Gainaru, C.; Böhmer, R. *Macromolecules* **2010**, ASAP (DOI: 10.1021/ma901805c).
(51) Ding, Y.; Kisliuk, A.; Sokolov, A. P. *Macromolecules* **2004**, *37*, 161–166.
(52) Abou Elfadl, A.; Herrmann, A.; Rössler, E. A., to be published.
(53) Fox, T.; Flory, P. J. *J. Polym. Sci.* **1954**, *14*, 315–319.
(54) Abou Elfadl, A.; Herrmann, A.; Hintermeyer, J.; Petzold, N.; Novikov, V. N.; Rössler, E. A. *Macromolecules* **2009**, *42*, 6816–6817.
(55) Ding, Y.; Sokolov, A. P. *Macromolecules* **2006**, *39*, 3322–3326.
(56) Herrmann, A.; Kariyo, S.; Abou Elfadl, A.; Meyer, R.; Novikov, V. N.; Rössler, E. A. *Macromolecules* **2009**, *42*, 5236–5243.
(57) Doi, M. *J. Polym. Sci., Polym. Phys. Ed.* **1983**, *21*, 667–684.
(58) Abdel-Goad, M.; Pyckhout-Hintzen, W.; Kahle, S.; Allgaier, J.; Richter, D.; Fetters, L. J. *Macromolecules* **2004**, *37*, 8135–8144.
(59) Chavez, F. V.; Saalwächter, K. **2010**, manuscript submitted.
(60) Adachi, K.; Yoshida, H.; Fukui, F.; Kotaka, T. *Macromolecules* **1990**, *23*, 3138–3144.